



Research paper

Modelling the effect of layer strength distribution on the brick-and-mortar failure regimes and properties

Georgia Hunter^a, Lee Djumas^a, Andrey Molotnikov^{a,b}, Laurence Brassart^{a,c,*}^a Department of Materials Science and Engineering, Monash University, Clayton, Australia^b RMIT Centre for Additive Manufacturing, School of Engineering, RMIT University, Melbourne, Australia^c Department of Engineering Science, University of Oxford, Oxford, UK

ARTICLE INFO

Keywords:

Nacre
Fracture mechanisms
Microstructural randomness
Micromechanical modelling
Composites

ABSTRACT

Brick-and-Mortar structures are of high interest because their staggered multi-material arrangement can result in a remarkable combination of high strength and high toughness. Synthetic replication of these structures with high geometric control has been made possible recently with the advances in multi-material Additive Manufacturing (AM). However, very little is known on how inherent material variation in the constituent materials, which can be significant in AM, affects the structure response.

In this work, we use a semi-analytical model to theoretically show that a variation in the strength of the layers in a Brick-and-Mortar structure has a significant effect on the failure response of the structure. It can lead to changes in failure regimes and negatively impact the mechanical properties, such as decrease the strain to failure or decrease the yield stress. This is particularly pronounced when the material behaviour is situated close to the transition point between failure regimes. We then present an experimental method to capture strength variability in the layer material and demonstrate that the incorporation of this variability into the semi-analytical model improves our prediction of the failure response of the structure, as compared to experiments.

1. Introduction

The mechanical properties of composites can be greatly influenced by variations in the microstructure. These variations can exist in both *material* properties and *geometric* properties and can affect the failure response and important mechanical properties, such as strength, toughness and strain to failure. The design of composite materials with superior mechanical properties therefore requires an in depth understanding of the effect of microstructural variations on the mechanical response of the structure.

One class of composites that has gained a lot of interest is the Brick-and-Mortar structure, which is inspired by the design motif observed in mollusk nacre shells. The Brick-and-Mortar structure consists of stiff bricks staggered with respect to one another and connected with a soft interfacial material between the bricks (subsequently referred to as the 'soft layer', or simply 'layer' for conciseness). These structures are found to be attractive due to their superior mechanical properties, exhibiting both high strength and high toughness (Barthelat et al., 2006, 2007a, 2007b; Dimas et al., 2013). Extensive studies have attempted to quantify a relationship between the geometric and material parameters of the

structure and its mechanical response to find the optimal parameters for strength and toughness. This includes the investigation of parameters such as brick aspect ratio (Begley et al., 2012; Hunter et al., 2021), brick shape (Hunter et al., 2022; Askarinejad et al., 2018), mineral inclusions (Askarinejad et al., 2021), nano-asperity inclusions (Askarinejad et al., 2015) and respective material properties of the bricks and layers (Begley et al., 2012; Hunter et al., 2021). Considerable work has also gone into understanding how geometric variation and stochasticity affects the properties of the Brick-and-Mortar structure (Yang et al., 2019; Abid et al., 2018, 2019; Zhang et al., 2010; Pro et al., 2015; Chintapalli et al., 2014; Bekah et al., 2012). This is because nacre (Barthelat et al., 2007a; Song et al., 2003) and early synthetic replication techniques (Launey et al., 2009; Munch et al., 2008; Deville et al., 2006; Oner Ekiz et al., 2009; Oaki et al., 2005; Gehrke et al., 2005; Wang et al., 2000; Bonderer et al., 2010a, 2010b), showed a variation in geometric properties in its structure.

The advances in multi-material Additive Manufacturing (AM) enabled a new possibility of manufacturing Brick-and-Mortar structures (Dimas et al., 2013, 2014; Djumas et al., 2016; Slesarenko et al., 2017a, 2017b; Gu et al., 2016, 2017a, 2017b; Mirzaeifar et al., 2015; Frølich

* Corresponding author. Department of Engineering Science, University of Oxford, Oxford, UK.

E-mail address: laurence.brassart@eng.ox.ac.uk (L. Brassart).

<https://doi.org/10.1016/j.mechmat.2023.104820>

Received 23 August 2022; Received in revised form 7 September 2023; Accepted 3 October 2023

Available online 14 October 2023

0167-6636/© 2023 The Authors. Published by Elsevier Ltd. This is an open access article under the CC BY license (<http://creativecommons.org/licenses/by/4.0/>).

et al., 2017; Zhang et al., 2015). This method has a high geometric control which removes the uncertainty in properties associated with geometric features. However, another form of variability still exists in the material properties of the constituent materials. For example, two of the materials printable with Material Jetting, which is an AM technique commonly used to manufacture Brick-and-Mortar structures, are reported by the manufacturer to have a tensile strength in the range of 50–65 MPa for VeroWhitePlus (VW+) (Vero Material Datasheet) and 0.8–1.5 MPa for TangoBlackPlus (TB+) (TangoPlus Datasheet). Although the manufacturer does not elucidate where this variability comes from, studies have shown that variability arises for structures printed in different orientations (Barclift et al., 2012; Cazón et al., 2014; Mueller et al., 2015; Kęsy et al., 2010; Bass et al., 2016), in different locations on the build tray (Mueller et al., 2015), with different spacing between parts (Mueller et al., 2015), when tested at different temperatures (Khalid et al., 2020) and when tested at different lengths of time after the printing of the part (Bass et al., 2016). However, even between replicate samples with the same printing parameters a strength variability of between 1.24% and 10.8% (Barclift et al., 2012) for VW+ and 5.56% (Libonati et al., 2016) and 9.8% (Khalid et al., 2020) for TB+ has been reported, indicating there is still an unknown inherent part of the printing process that can cause variations in property.

The variation observed in the strength of these AM materials therefore raises the question of how material variability affects the mechanical response of Brick-and-Mortar structures. Very few studies have explored this question. In one study, layer variability was included by the random removal of layers throughout the structure (Anup, 2015). Here, the removal of layers is predicted to decrease the stiffness, toughness and strength, demonstrating that material variation in the layers does have a significant effect on the composite response. This study is limited, however, by an ‘all-or-nothing’ approach where layers either exist or are removed. Another series of studies (Luo et al., 2017, 2018) have used a statistical fishnet model (a system of tensile diagonal links) to show that the probability of failure of the Brick-and-Mortar structure is lower than the probability of failure of its constituent materials. One limitation in this study is that only the shear layers (horizontal layers) are modelled. A more recent study (Yan et al., 2022) incorporated the normal layers (vertical layers) and separately assigned a strength to each normal and shear layer based on a Weibull distribution. In this case, the maximum strength of the structure was shown to decrease in magnitude, and increase in variation, with increasing variation in the layer material strength. This study highlights the importance of incorporating the degree of the material variation into models of Brick-and-Mortar structures to accurately predict their overall strength. One limitation in this study, however, is the limited range of parameters tested. Specifically, all the structures explored in the study exhibited a single failure regime (see below). Notably, none of the aforementioned studies that numerically or analytically investigate the effect of material variability on Brick-and-Mortar structures attempted to compare modelling predictions to experimental data.

In our recent study (Hunter et al., 2021), we identified two distinct ‘layer-only’ failure regimes for Brick-and-Mortar structures, which are dependent on the geometric and material parameters. The two failure types are differentiated by how well they distribute damage prior to failure whereby ‘two-peak’ failure is unable to distribute damage prior to failure and ‘peak-plateau-peak’ failure distributes damage throughout all the normal layers prior to failure. Control of these regimes is a key to tailoring the response of these structures. Specifically, it was shown that the ‘peak-plateau-peak’ failure regime is superior to the ‘two-peak’ regime, exhibiting higher toughness without compromising strength. The structures utilised in the studies that explore the effect of material variability (Anup, 2015; Yan et al., 2022) all fall within the ‘two-peak’ failure regime, where damage is not distributed throughout the normal layers of the structure prior to failure.

In the present paper, we aim to develop a more complete map of the effect of material variation on the Brick-and-Mortar structure by

exploring a larger parameter space that covers both failure regime types, as well as explore how variation affects the failure regime exhibited by the structure. A theoretical study is conducted to explore the effect of layer strength variability on the failure response of the Brick-and-Mortar structure for sets of geometric and material parameters that span both failure regimes. To do this, we rely on our previously derived semi-analytical model for finite-sized structures representative of additive manufactured structures (Hunter et al., 2021). Different from previous approaches, our model incorporates both the normal and shear layers and has been shown to capture the two different ‘two-peak’ and ‘peak-plateau-peak’ failure regimes for the first time. Here, we extend our model by assigning a strength value to each layer of the Brick-and-Mortar structure based on a normal distribution. The resulting stress-strain response, the failure regimes exhibited and the key failure properties are investigated, including the yield stress (indicative of first failure) and the strain to failure (indicative of final failure). We then compare modelling predictions to experimental data and demonstrate that the incorporation of variability improves the prediction of the mechanical and failure response of Brick-and-Mortar structures.

The model is described in Section 2, and model predictions are presented in Section 3. The experimental Proof-of-Concept is presented in Section 4, before concluding.

2. Semi-analytical model

2.1. Model without a distribution

In our previous work (Hunter et al., 2021), we developed a semi-analytical model for rectangular Brick-and-Mortar structures under uniaxial tension. The structure is considered as a finite-size system of N_C unit cells in the (horizontal) loading direction, see Fig. 1. Uniform horizontal displacements are applied on the right boundary of the domain, and zero horizontal displacements are applied on the left boundary. Periodic boundary conditions are considered in the vertical direction while preventing vertical rigid body motion. Continuity of the mechanical fields (forces and displacements) in bricks and normal layers shared between two adjacent unit cells is considered. Here the number of unit cells (and hence the number of bricks) is kept relatively small for the geometry to be representative of additive manufactured Brick-and-Mortar structures, where the number of bricks typically is of the order of tens. We note that Statistical Volume Elements (SVEs) of structures with an ‘infinite’ number of brick can also be obtained within our framework by considering a very large number of unit cells and bricks of the order of thousands (Abid et al., 2018, 2019). However, such SVEs can hardly be produced by additive manufacturing.

In this setup, there are three types of geometric entities: bricks, shear layers (layers parallel to the loading direction) and normal layers (layers perpendicular to the loading direction). In the analysis, bricks are assumed to be rigid and the layers’ response is described using a Cohesive Zone Model (CZM) with bilinear traction-separation law, thus incorporating the deformation and damage response of the layer simultaneously.

The traction separation law of the layers is defined via the following parameters: an effective normal modulus (E_n), a normal strength (σ_{max}), a normal fracture energy (G_{IC}), an effective shear modulus (E_s), a shear strength (τ_{max}), and a shear fracture energy (G_{IIC}). The traction separation law relates the opening displacement of the layers to the stress in the layer as follows:

$$\sigma = E_n \frac{d_n}{t} \quad (1)$$

$$\tau = E_s \frac{d_s}{t} \quad (2)$$

where σ is the normal stress in the normal layer and d_n its opening displacement, τ is the shear stress in the shear layer and d_s its opening

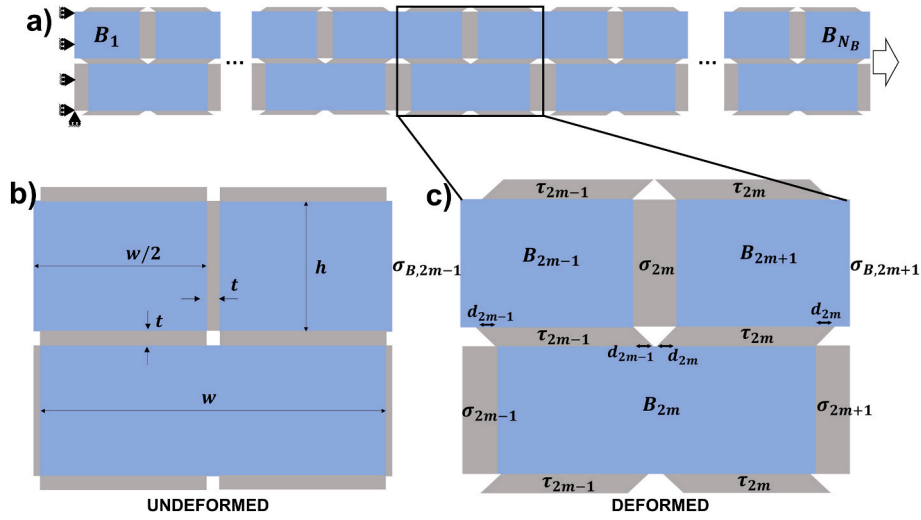


Fig. 1. a) Schematic representation of the finite-sized representative geometry of the Brick-and-Mortar structure with a finite number N_C of unit cells, corresponding to a finite number $N_B (= 2N_C + 1)$ of rigid bricks. The structure is shown in its deformed state. b) A single unit cell is included to show the structure in its undeformed state and to identify the nomenclature used to define the geometric parameters of the structure. c) A second unit cell is included to show the structure in its deformed state and to highlight the nomenclature used to define the brick number, the stresses in the layers and the displacement between adjacent bricks in its deformed state.

displacement. E_n^* and E_s^* represent damaged normal and shear modulus, respectively, and are given by:

$$E_n^* = E_n(1 - D_n), E_s^* = E_s(1 - D_s) \quad (3)$$

where D_n and D_s are damage variables that evolve monotonically from 0 to 1 once the strength of the normal or shear layer, respectively, is reached.

In the multi-cell Brick-and-Mortar construct, each layer is assigned its own set of parameters which can be separately controlled, and is denoted as follows: the i th shear layer is assigned the parameters $E_{s,i}$, $\tau_{max,i}$, $G_{IC,i}$ and the i th normal layer is assigned the parameters $E_{n,i}$, $\sigma_{max,i}$, $G_{IC,i}$.

As derived in our previous work, the relative displacement between each brick for a system of N_C juxtaposed unit cells with known prescribed displacement d_T (corresponding to a composite strain of $\epsilon_T = d_T/(w + t)$), is determined by solving the following set of equations:

$$-(2E_{n,1}^*h + E_{s,1}^*w)d_1 + (E_{n,3}^*h + E_{s,2}^*w)d_2 + E_{n,3}^*hd_3 = 0 \quad (4)$$

$$-E_{n,i}^*hd_{i-1} - (E_{n,i}^*h + E_{s,i}^*w)d_i + (E_{n,i+2}^*h + E_{s,i+1}^*w)d_{i+1} + E_{n,i+2}^*hd_{i+2} = 0, \quad i = 2, 3, \dots, 2N_C - 2$$

$$-E_{n,2N_C-1}^*hd_{2N_C-2} - (E_{n,2N_C-1}^*h + E_{s,2N_C-1}^*w)d_{2N_C-1} + (2E_{n,2N_C+1}^*h + E_{s,2N_C}^*w)d_{2N_C} = 0$$

$$d_T = \sum_{i=1}^{2N_C} d_i$$

With the known displacements, the stress in each of the normal (σ_i) and shear (τ_i) layers, respectively can be determined from:

$$\sigma_i = \begin{cases} \frac{2E_{n,i}^*d_i}{t}, & i = 1 \\ \frac{E_{n,i}^*(d_{i-1} + d_i)}{t}, & i = 2, 3, \dots, 2N_C \\ \frac{2E_{n,i}^*d_{i-1}}{t}, & i = 2N_C + 1 \end{cases} \quad (5)$$

$$\tau_i = \frac{E_{s,i}^*d_i}{t}, \quad i = 1, 2, \dots, N_C \quad (6)$$

The macroscopic stress for the prescribed strain can then be calculated on the loading edge, as:

$$\sigma_C = \frac{\sigma_{2N_C}h + \tau_{2N_C}w + \sigma_{2N_C+1}h}{2h} \quad (7)$$

Note that there are no intrinsic size effects in the model. The geometry is completely characterised by the brick aspect ratio $A_R = w/h$ and the brick height to layer thickness ratio h/t .

In our previous work, we introduced a small defect into one of the layers to trigger localised damage by reducing the strength of a single

layer by a very small amount (0.1%) and demonstrated that two different failure mechanisms arise, dependent on whether the structure can distribute the damage to the rest of the structure ('peak-plateau-peak' failure) or if it fails immediately through the shear layers ('two-peak' failure). In this work, we utilise the ability to control each layer separately to introduce a strength distribution to the layers.

2.2. Microstructural randomness

To investigate the effect of a distribution in the strength of the layer

material on the properties of the Brick-and-Mortar structure, the strength of the layer material is defined by a normal distribution:

- The strength of the normal layers (σ_{max}) are defined by an average maximum strength ($\bar{\sigma}_{max}$) and a standard deviation (σ_{sd}) which is a proportion (p_n) of the average maximum strength: i.e. $\sigma_{sd} = p_n \bar{\sigma}_{max}$.
- The strength of the shear layers (τ_{max}) are defined by an average maximum strength ($\bar{\tau}_{max}$) and a standard deviation (τ_{sd}) which is a proportion (p_s) of the average maximum strength: i.e. $\tau_{sd} = p_s \bar{\tau}_{max}$.

We adopted a normal distribution for simplicity, assuming that the layer strength distribution arising from the AM process is distributed symmetrically around a mean value. As shown in the following, using a normal distribution is sufficient for a proof-of-concept illustrating the effect of strength distribution on the properties of Brick-and-Mortar structures, and reasonably well captures the experimental trends. Other distributions could of course be considered, however this is outside the scope of this paper.

To implement this distribution into the finite-size semi-analytical model, each layer in the structure is separately assigned a strength value using an inbuilt normal distribution random number generator ('normrnd' in MATLAB): i.e., each normal layer was randomly assigned a maximum strength value ($\sigma_{max,i}$) based on the normal distribution with an average of $\bar{\sigma}_{max}$ and a standard deviation of σ_{sd} , while each shear layer was randomly assigned a maximum strength value ($\tau_{max,i}$) based on the normal distribution with an average of $\bar{\tau}_{max}$ and a standard deviation of τ_{sd} .

The first sets of simulations (sections 3.1-3.6) were run with $N_c = 10$ unit cells to capture a relatively small finite-size structure representative of the size of Brick-and-Mortar structures realistically printable with Additive Manufacturing, such as the structures considered in Section 4. For completeness, we also present a study in section 3.7 to investigate the effect of size (via the number of unit cells) on the failure regimes and mechanical properties of a Brick-and-Mortar structure with layer strength variability. Due to the random assignment of strength values in the layers, different simulations for the same strength distribution may result in a different response. Therefore, multiple simulations (100) were run for each parameter set with a distribution. Key properties, such as yield stress and strain to failure, were extracted by calculating the average and standard deviation of these properties from the 100 simulations.

3. Parametric study

3.1. Stress-strain response without layer variation

Before considering the effect of layer strength distribution on the failure response of Brick-and-Mortar structures, we first present the two types of stress-strain response for the structures without a distribution,

see Fig. 2. As shown in our previous work (Hunter et al., 2021), there are distinct failure events in a Brick-and-Mortar structure, which relate to the type of failure regime exhibited:

- The first peak, which corresponds to the yield stress, is dictated by the first layer to fail. The conditions for the shear layers to fail first ('called 'shear-only' failure), include a combination of a very stiff, but weak shear layers and very strong normal layers (Hunter et al., 2021). This is an unusual combination and therefore the normal layer will generally be predicted to fail first.
- After the first normal layers have failed, the structure will either be able to distribute damage to more normal layers, or it will fail in the shear layer that is between the already failed normal layers. If it fails in the shear layer, then the structure exhibits 'two-peak' (tp) failure, see Fig. 2a. If it can distribute damage to more normal layers, then it will enter a plateau region in the stress-strain response. If it successfully distributes damage to all normal layers before the shear layers fail then it exhibits 'peak-plateau-peak' (ppp) failure and has a significantly increased strain to failure compared to 'two-peak' failure, see Fig. 2b. We attribute the random zigzag pattern in the plateau region to the semi-analytical nature of the model, i.e. to the numerical round-off errors when solving the linear system of equations, which are responsible for triggering failure of layers randomly.
- If the structure fails while it is within the plateau region, then the structure is at the transition between the two failure regimes. For this paper, we will call this type of failure 'peak-plateau' (pp) failure. Note that this regime is not predicted in the semi-analytical model for a structure without a distribution, however it will be a possible regime once a distribution is considered.

Also presented in our previous work (Hunter et al., 2021), the failure regime for a structure with geometric parameters of $A_R = w/h$ (aspect ratio) and material parameters of $E_R = E_n/E_s$ (relative normal-to-shear effective moduli) and $\sigma_R = \tau_{max}/\sigma_{max}$ (relative shear-to-normal layer strength) is determined by a dimensionless variable f_r :

$$f_r = \frac{\sigma_D}{\sigma_R}, \text{ where } \sigma_D = \left(\frac{1}{2E_R} + \frac{1}{A_R} + \frac{1}{2(E_R + A_R)} \right) \quad (8)$$

where σ_D is representative of the ratio of the stress in a shear layer joining the first two adjacent normal layers to fail and the stress in the next adjacent intact normal layer. The dimensionless variable can be used to determine the failure regime, for a structure without a distribution, as follows:

- If $f_r > 1$ (i.e. σ_D is larger than σ_R) the shear layer reaches its strength before the normal layer reaches its strength. This results in failure of the shear layer before any more normal layers fail, which is indicative of 'two-peak' failure.

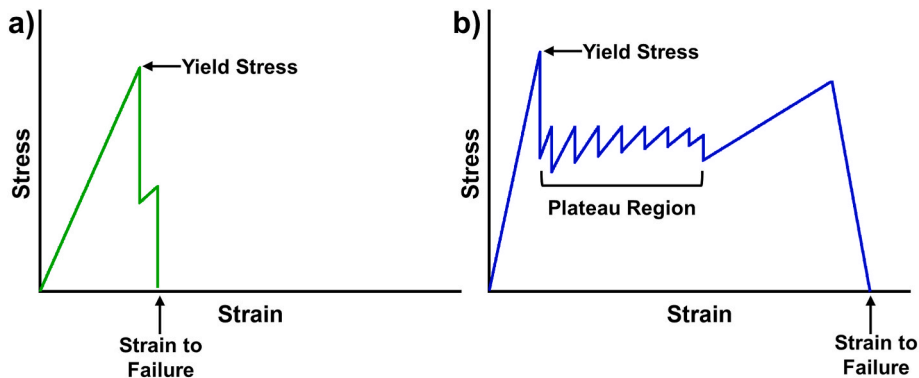


Fig. 2. Schematic of the stress-strain response for a) 'two-peak' failure and b) 'peak-plateau-peak' failure, showing key points in the failure response.

Table 1

Geometric and material parameters used in the analysis.

σ_R	E_R	h/t	N_C
0.33	10	8	10

- If $f_r < 1$ (i.e. σ_D is smaller than σ_R) than the next adjacent intact normal layer reaches its strength before the shear layer. This results in propagation of the damage through the normal layers of the structure prior to failure of the shear layers, which is indicative of ‘peak-plateau-peak’ failure.
- If $f_r = 1$ (i.e. σ_D is equal to σ_R) then the structure is at the transition point between the two regimes.

The magnitude of f_r is also important, as it quantifies how large the difference in shear layer-to-normal layer stress (σ_D) is compared to the shear-to-normal strength (σ_R). Therefore, an f_r value that is further away from 1 is further away from the transition point between failure regimes.

3.2. Stress-strain response with layer variation

We now consider the effect of layer strength distribution on the response of Brick-and-Mortar structures. To test the effect of layer strength distribution on different failure regimes, three different aspect ratios of 3, 4.5 and 6 were first considered with all other geometric and material parameters kept constant, see Table 1. These aspect ratios were chosen because, for the set material parameters and according to Equation (8), an A_R of 3 corresponds to ‘two-peak’ failure ($f_r = 1.27$), an A_R of 6 corresponds to ‘peak-plateau-peak’ failure ($f_r = 0.74$) and an A_R of 4.5 is just above the transition point (within the ‘peak-plateau-peak’ region) between regimes ($f_r = 0.94$). Simulating these three aspect ratios therefore allows us to differentiate the respective effect of a distribution in the layer strength on the different failure regimes.

The resulting stress-strain responses for each A_R structure with a distribution introduced into 1) the normal layers only ($p_n = 0.1$ and $p_s = 0$), 2) the shear layers only ($p_n = 0$ and $p_s = 0.1$) and 3) both the normal and shear layers concurrently ($p_n = 0.1$ and $p_s = 0.1$), is shown in Fig. 3. The type of failure regime exhibited by each of the 100 simulations for

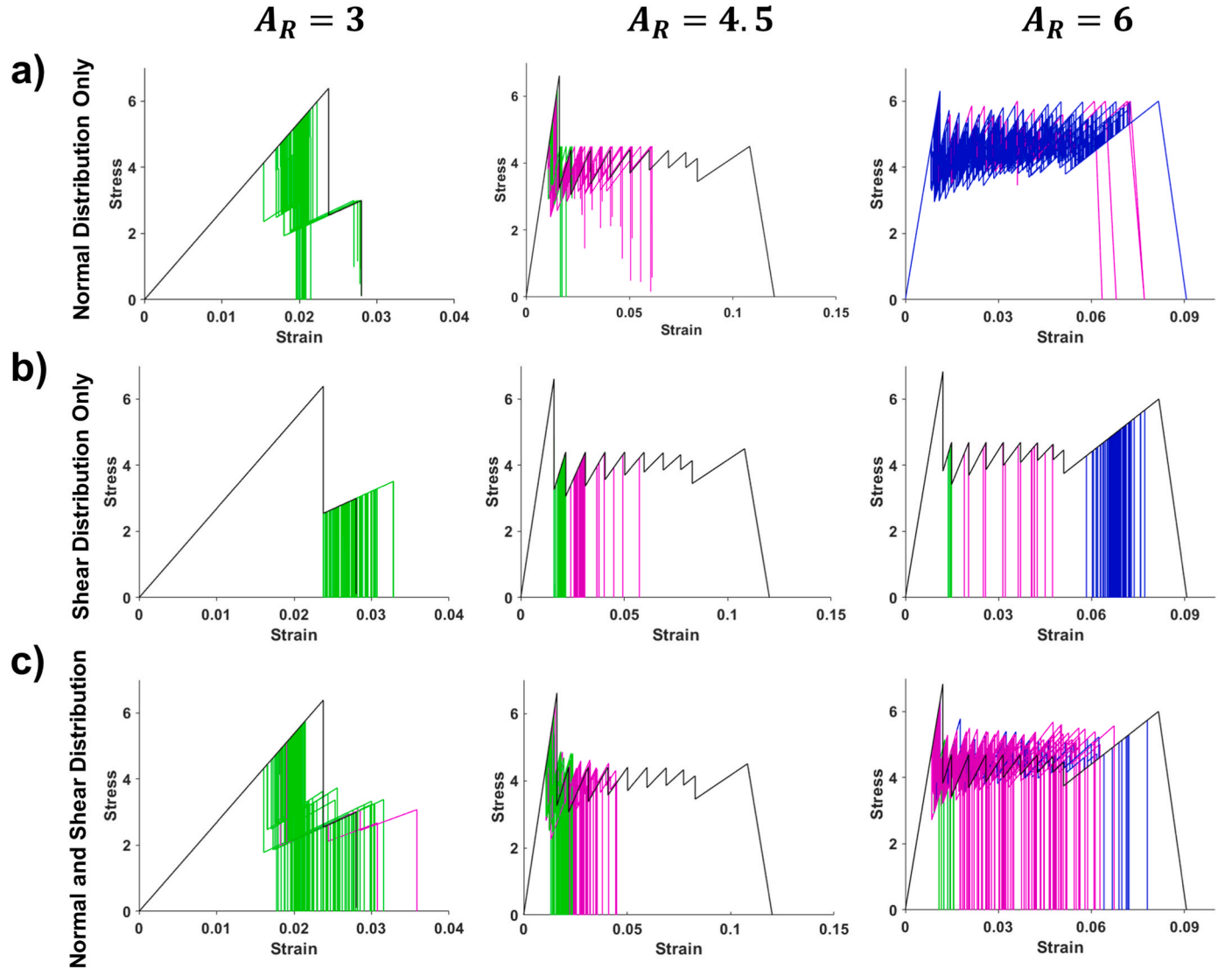


Fig. 3. Stress-strain response for three different aspect ratios with a distribution in the a) normal layers only ($p_n = 0.1, p_s = 0$), b) the shear layers only ($p_n = 0, p_s = 0.1$), and c) the normal and shear layers concurrently ($p_n = p_s = 0.1$). The colours correspond to the type of failure regime exhibited: blue corresponds to ‘peak-plateau-peak’ failure, purple corresponds to ‘peak-plateau’ failure and green corresponds to ‘two-peak’ failure. The response of each structure without a strength distribution in the layers is also included in black for comparison. (For interpretation of the references to colour in this figure legend, the reader is referred to the Web version of this article.)

each parameter set is visually represented in the stress-strain plots by colour: green represents ‘two-peak’ failure, purple represents ‘peak-plateau’ failure and blue represents ‘peak-plateau-peak’ failure. The stress-strain response of the structure without a layer strength distribution is also included in each plot in black for comparison.

3.3. Effect of layer variation on the failure regime

An important trend that is observed in Fig. 3 is that structures that are initially (i.e. prior to introducing a distribution in properties) in the ‘peak-plateau-peak’ failure regime are showing a probability of dropping down to ‘peak-plateau’ or ‘two-peak’ failure with the introduction of a distribution. The probability is observed to be highest for the structure that is very close to the transition point (i.e. A_R of 4.5).

To validate this trend for a broader range of distribution sizes and f_r values, a range of p_n and p_s values were simulated for the same three aspect ratios plus two additional aspect ratios: an A_R of 7.5, corresponding to an f_r value of 0.64 and therefore ‘peak-plateau-peak’ failure

without a distribution, and an A_R of 1.5, corresponding to an f_r value of 2.28 and therefore ‘two-peak’ failure without a distribution.

The proportion of simulations for each parameter set that exhibit each type of failure regime were tracked and are plotted in a stacked histogram for effective comparison between the structures of different variation size, different f_r value and different distribution type (i.e. normal only, shear only and concurrent shear and normal distribution), see Fig. 4.

Here we confirm that structures that are initially in the ‘peak-plateau-peak’ failure regime (i.e. without a distribution) can show a probability of dropping down to ‘peak-plateau’ or ‘two-peak’ failure with the introduction of a distribution. From these plots we further observe that a certain size distribution is required for the structure to drop down to these failure regimes, and the size of this variation increases the further away the structure is from the transition point (i.e. the further away f_r is from 1). For example, when there is concurrently a variation in both the shear and normal layers, a variation of p_n and p_s of 0.01, 0.1 and 0.2 is required for structures with f_r value of 0.92, 0.74 and

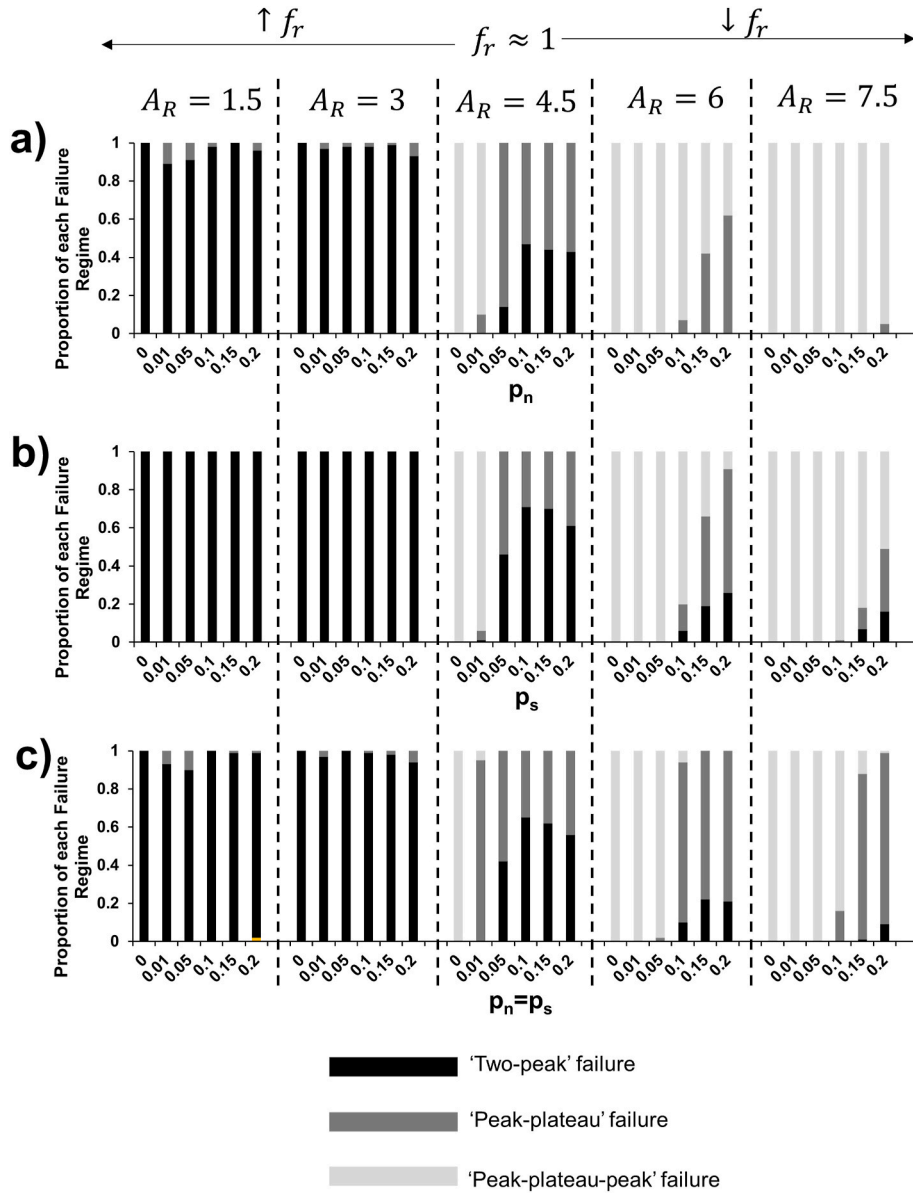


Fig. 4. Proportion of structures that exhibit each failure regime for a range of aspect ratios (corresponding to a range of f_r values), for a range of distribution sizes and for a distribution in a) normal layers only, b) shear layers only and c) both the normal and shear layers concurrently. Proportions are taken from 100 simulations for each combination of A_R , distribution size and distribution type.

0.64, respectively.

We also identify from these plots that a distribution in either the normal or shear layers can cause the failure regime to drop down to these failure regimes, although the shear layers exhibit a higher sensitivity to a change in failure regime. Interestingly, when there is a distribution in both the shear and normal layers concurrently, the probability of exhibiting a different failure regime is highest, suggesting variations in the respective normal and shear layers have an ‘additive’ effect on the variation in the failure regime.

3.4. Effect of layer variation on the yield stress

A distribution in the layers also affects the yield stress, see Fig. 3, which is indicative of the first layer to fail. The yield stress is noticeably decreased with the introduction of a strength distribution in the normal layers for all structures and is not affected by a strength distribution in the shear layers. The yield stress is negatively affected by a distribution in the normal layers because the yield stress is dictated by the first normal layer to fail, which is dictated by the weakest normal layer, and a larger normal layer strength distribution results in a higher probability of weaker normal layers. The yield strength is not affected by a strength distribution in the shear layers because it is the normal layers that fail first and therefore a distribution of strength in the shear layers does not affect the yield stress. Significantly, this is different from observations reported in the literature, which have shown that a distribution in shear layer strength affects the structure strength. This apparent contradiction exists because in previous studies either 1) normal layers are not included in the model of the structure (Luo et al., 2017, 2018) or 2) it is the maximum strength and not the yield strength that is tracked (Yan et al., 2022). In contrast, our study demonstrates that a strength distribution within the normal layers does have a significant effect on the yield stress, and therefore that normal layers need to be taken into account to accurately describe the behaviour of Brick-and-Mortar

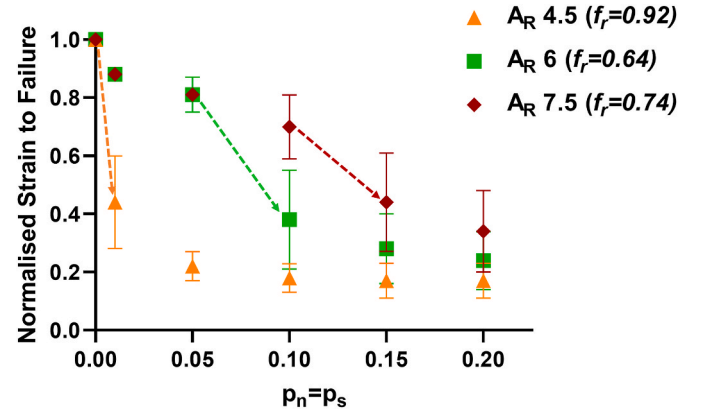


Fig. 6. Comparison of normalised strain to failure (average and standard deviation) for the range of aspect ratios with $f_r < 1$ and for a range of $p_n = p_s$ distributions. Here, the results of each structure are normalised by the strain to failure of a structure with the same A_R and without a distribution in the strength of the layers. The dashed lines correspond to the transition from when the structure exhibits predominantly ‘peak-plateau-peak’ failure to when the structure has a significant probability of ‘peak-plateau’ and/or ‘two-peak’ failure.

structures.

A plot of the normalised yield stress for the broader range of distributions and aspect ratios tested is shown in Fig. 5 and quantitatively validates this trend. (Note that the yield stress for each structure is normalised by the yield stress of the equivalent structure without a distribution in layer strength). This plot further illustrates that the decrease in normalised yield stress is equivalent across all structures, regardless of its aspect ratio and regardless of its failure regime type.

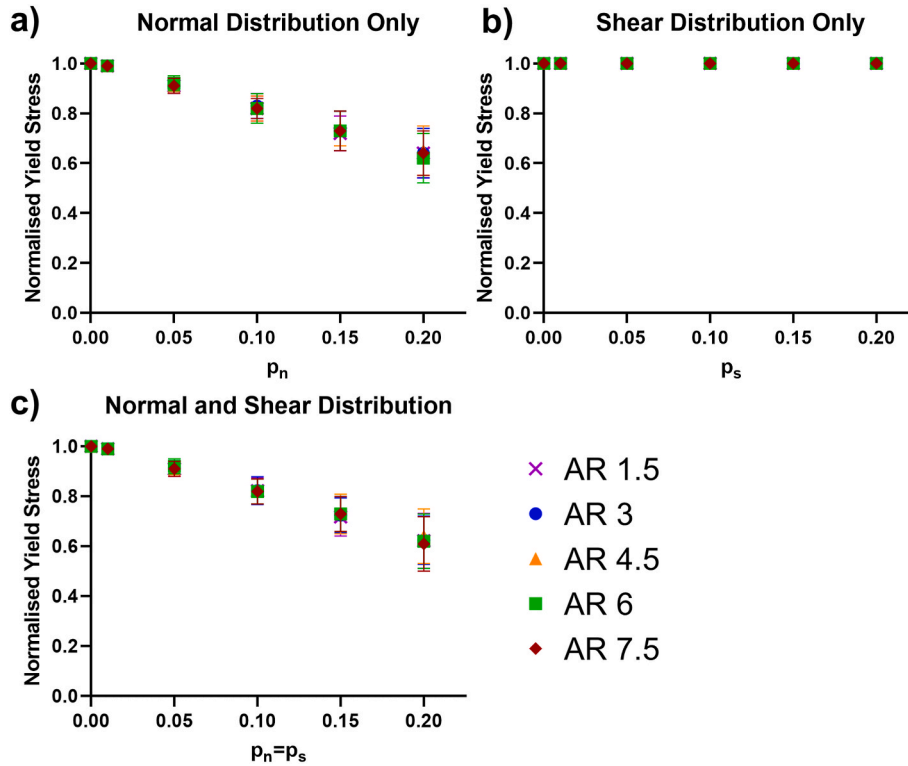


Fig. 5. Effect on the normalised yield stress of a strength distribution in a) the normal layers, b) the shear layers and c) both the normal and shear layers concurrently, for a range of aspect ratios. Here, the results of each structure are normalised by the yield stress of a structure with the same A_R and without a distribution in the strength of the layers.

3.5. Effect of layer variation on the strain to failure

The change in failure regime type with the introduction of a distribution does not affect the yield stress; however, it does appear to affect the strain to failure. From Fig. 3 we visually observe that the strain to failure decreases in value and increases in variation when there is a probability of a change in failure regime.

A plot of the normalised strain to failure for the broader range of distributions and aspect ratios tested, see Fig. 6, quantitatively validates this trend. (Note that the strain to failure for each structure is normalised by the strain to failure of the equivalent structure without a distribution in layer strength). Here we observe a significant decrease in normalised strain to failure at the variations in layer strength that correspond to a

probability of a change in failure regime of the structure. The transition to a probability of different failure regimes, as identified in Fig. 4, is represented by dashed lines in the strain to failure plot. At this same point, we also see a significant increase in the variation of the strain to failure, as indicated by the increase in the standard deviation which are captured by error bars in the plot. Note that here we show the plot corresponding to concurrent normal and shear layer variation, however the same general trends are observed for shear-only and normal-only distributions.

3.6. Comparing the effect of material and geometric parameters

In the previous sections, the aspect ratio was used to control the

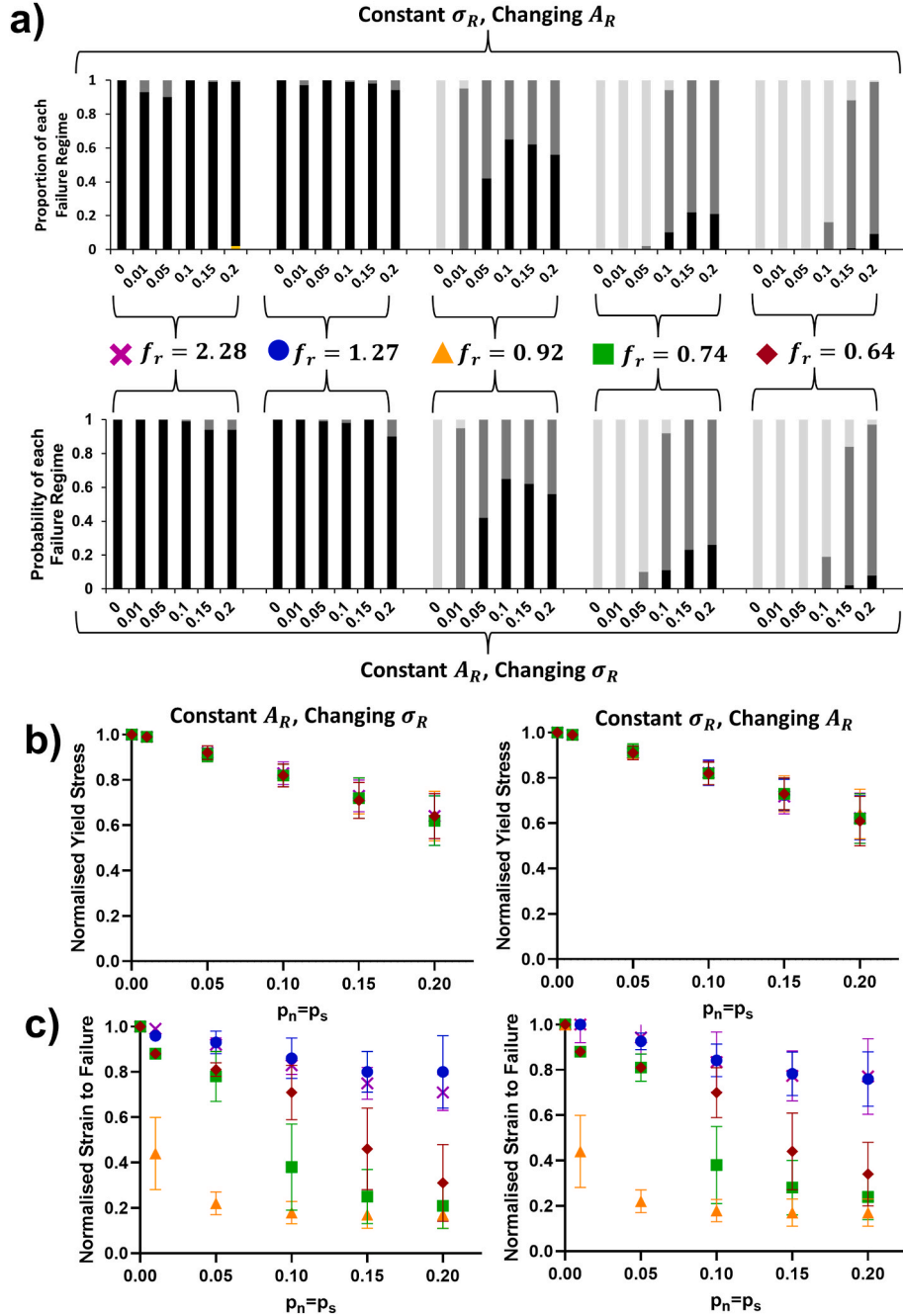


Fig. 7. Comparison of the effect of a distribution in the normal and shear layer strength on the probability of each a) failure regime (different shades of grey represent different failure regimes, the same as in Fig. 4), b) normalised strain to failure and c) normalised yield stress for structures with the same f_r value, but with different σ_R and A_R combinations. (For interpretation of the references to colour in this figure legend, the reader is referred to the Web version of this article.)

failure regime in the absence of a distribution. However, the relation that determines which failure regime is exhibited (without a distribution) is also dependent on the relative shear-to-normal layer properties, see Equation (8). In this section, we explore whether the layer strength distribution has a different effect on the structure response if the original failure regimes are controlled by the normal and shear layer properties, compared to if it is controlled by the aspect ratio. To do this, a range of σ_R values were tested for a constant A_R of 4.5. For effective comparison of the effect of changing the aspect ratio to the effect of changing the respective normal-to-shear layer strength, the σ_R values that were tested were chosen to have the same f_r values that were tested for changing A_R : i.e. $\sigma_R = 0.135, 0.24, 0.33, 0.41, 0.5$, corresponding to $f_r = 2.28, 1.27, 0.92, 0.74$ and 0.64 , respectively.

Remarkably, it was found that the effect on the failure regime, normalised strain to failure and normalised yield stress is the same for structures that have the same f_r value, see Fig. 7. This observation is significant as it demonstrates that the failure response of the structure is quantitatively dependent on the combination of material and geometric parameters, as defined by the dimensionless parameter f_r (Equation (8)).

3.7. Effect of number of unit cells

It is a well-known phenomenon ('weakest link statistics') that strength is affected by the size of a structure once strength variability or flaws are introduced into a structure. In this sub-section, we explore whether size also affects the failure regime of a Brick-and-Mortar structure once a layer strength distribution is introduced. We do this by testing structures with a range of sizes ($N_C = 2, 5, 10, 15, 20$) for the five aspect ratios tested in previous sections. All simulations in this section implement a constant size distribution in the normal and shear layer strength ($p_n = p_s = 0.1$).

For the structures with $f_r < 1$ (i.e. 'peak-plateau-peak' failure without a distribution) there is a clear increase in the proportion of structures that exhibit 'peak-plateau' or 'two-peak' failure with increasing size of the structure, see Fig. 8a. While for the structures with

$f_r > 1$ (i.e. 'two-peak' failure without a distribution) there is minimal change in the failure regime with changing structure size. The structures that exhibit an increase in probability of 'peak-plateau' and 'two-peak' failure regimes with increasing structure size also exhibit a decrease in normalised strain to failure with increasing structure size, see Fig. 8b. For these plots, each structure is normalised by the same size structure without a distribution and with the same geometric and material parameters. As expected from weakest link statistics, the normalised yield stress also decreases with increasing size for all structures, see Fig. 8c. These results indicate the importance of incorporating an accurate structure size when predicting the failure response and mechanical properties of a Brick-and-Mortar structures of small, finite-size, such as structures produced by Additive Manufacturing.

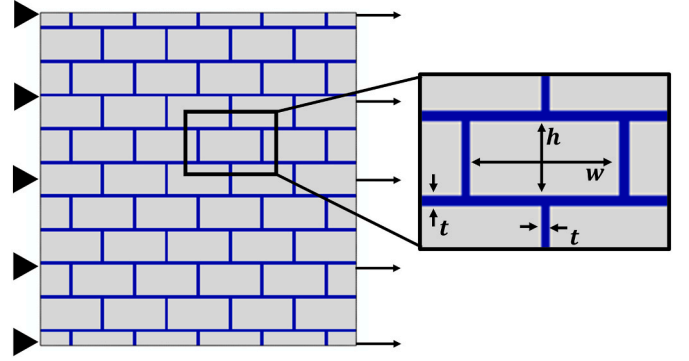


Fig. 9. Visual representation of the geometric parameters, structure size and loading conditions of the uniaxial tension tests of the Brick-and-Mortar structures.

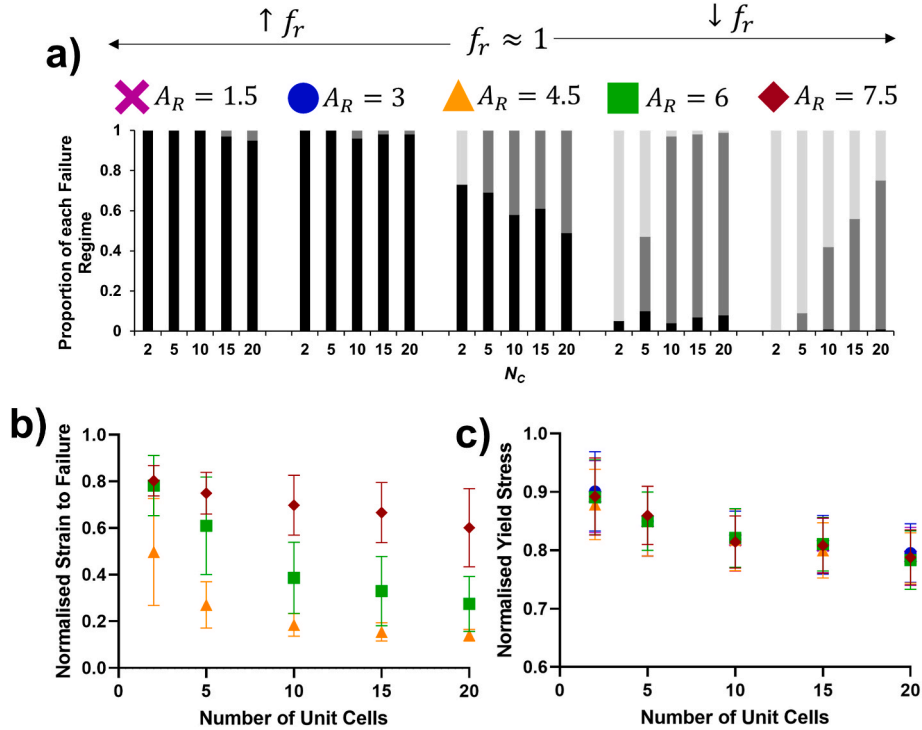


Fig. 8. The effect of structure size on a) the proportion of failure regimes exhibited by the structure (different shades of grey represent different failure regimes, the same as in Fig. 4), b) the normalised strain to failure and c) the normalised yield stress for a range of aspect ratios and with a strength variability in the normal and shear layers ($p_n = p_s = 0.1$). (For interpretation of the references to colour in this figure legend, the reader is referred to the Web version of this article.)

4. Experimental proof of concept

The previous section showed that the variability of the layer material can have a significant effect on the failure regime and the key failure properties for a Brick-and-Mortar structure. To demonstrate the practical importance of capturing layer strength variability in models of Brick-and-Mortar structures, we will experimentally show that the incorporation of variability improves our prediction of the failure response of Brick-and-Mortar structures.

To do this, we will first present a method to experimentally calibrate the CZM parameters for a layer with a strength distribution. We will then implement this strength variability into the semi-analytical model and compare the results to experimental uniaxial tests of Brick-and-Mortar structures with different aspect ratios taken from our previous work (Hunter et al., 2021). We will specifically use the experimental results of Brick-and-Mortar structures with A_R of 2.5, 4.5, and 6.1, respectively, as these ratios were experimentally shown to span the failure regimes. All experimentally tested structures in this previous work were fabricated with the Objet Connex500 3D printer (Stratasys, Ltd.) with TB + layers and VW + bricks and had structure size and loading conditions as shown in Fig. 9 (For further details on the methodology for these experiments, see (Hunter et al., 2021)).

4.1. Experimental calibration of strength variation in layer material

We presented a method for the calibration of the CZM parameters for the layer material of a Brick-and-Mortar structure in our previous work (Hunter et al., 2021). In this previous study, the normal and shear properties of the layer material (TB+) were experimentally determined using a Layered Tensile Test and a Single Lap Joint test, see schematic insets in the plots of Fig. 10, where the adherend was comprised of the same material as the bricks (VW+) and the adhesive has an area of 10×3.125 mm and a thickness of 0.25 mm. A single representative curve was then used to calibrate the CZM parameters.

In the current study, additional LTT and SLJ experiments were conducted to get a better spread of the mechanical response, and all the experimental results were used to calibrate the CZM parameters and to incorporate a strength distribution. The method to calibrate the CZM parameters with a strength distribution in this study was as follows:

- 1) The average force at yield (\bar{F}_Y), average displacement at yield (\bar{d}_Y) and average displacement at failure (\bar{d}_F) from all the experimental tests was determined.
- 2) The CZM parameters were calibrated by simulating the LTT and SLJ tests using Finite Element Analysis and adjusting the CZM parameters until the force at yield, displacement to yield and displacement to failure of the simulations matched \bar{F}_Y , \bar{d}_Y and \bar{d}_F , respectively. The LTT tests were used to calibrate the normal CZM parameters (σ_{max} , E_n ,

G_{IC}) while the SLJ tests were used to calibrate the shear CZM parameters (τ_{max} , E_s , G_{IIC}). In these simulations, the adherend was modelled by a linear elastic material with Young's Modulus of 1500 MPa and Poisson's ratio of 0.3 to capture the properties of the adherend, i.e. VW+ (Hunter et al., 2021).

- 3) To capture the distribution in the strength, the standard deviation in the strength of the experimental results was calculated. For the normal and shear layers the standard deviation in the strength corresponded to 10% of the average strength (i.e. $p_n = 0.1$ and $p_s = 0.1$). Therefore, a standard deviation corresponding to $p_n = 0.1$ and $p_s = 0.1$ was applied to the TB + CZM strength parameters to capture the distribution in the layer strength. For comparison, literature has reported a variation in the tensile strength of TB+ of 5.6% (Libonati et al., 2016), 9.8% (Khalid et al., 2020) and 22% (TangoPlus Data-sheet). Therefore, the 10% variation calculated in our results appears reasonable.
- 4) To determine the corresponding G_{IC} and G_{IIC} value for a particular strength value within the distribution, we note that these parameters can be rewritten in terms of strength, effective moduli and relative strain to yield and strain to failure (i.e. $\varepsilon_Y/\varepsilon_F$), as follows:

$$G_{IC} = \frac{\sigma_{max}^2 \varepsilon_F}{2E_n \varepsilon_Y} t \quad (9)$$

$$G_{IIC} = \frac{\tau_{max}^2 \varepsilon_F}{2E_s \varepsilon_Y} t \quad (10)$$

It is calculated that the relative displacement to yield and displacement to failure in the experiments is approximately constant for each sample type. This is calculated to correspond to a constant $\varepsilon_F/\varepsilon_Y = 1.23$ in the CZM model of the shear properties and $\varepsilon_F/\varepsilon_Y = 2.74$ in the CZM model of the normal properties. Substituting this into equations (9) and (10), we can therefore calculate the G_{IC} and G_{IIC} for a particular strength value. Note that we assume here that the effective modulus (E_n and E_s) remains constant as we observe only a very small variation in stiffness in the stress-strain response of the LTT and SLJ tests compared to the variation in strength, see grey curves in Fig. 10.

The resulting CZM parameters for TB+, including the resulting strength distribution, is provided in Table 2. A visual representation of the fitted strength distribution for the shear and normal properties is provided in Fig. 10.

Table 2
Calibrated CZM parameters with Strength Distribution.

	E_n	$\sigma_{max} \pm \sigma_{sd}$	G_{IC}	E_s	$\tau_{max} \pm \tau_{sd}$	G_{IIC}
TB+	14	6.7 ± 0.67	$\frac{2.74\sigma_{max}^2 t}{2E_n}$	1	2.55 ± 0.26	$\frac{1.23\tau_{max}^2 t}{2E_s}$

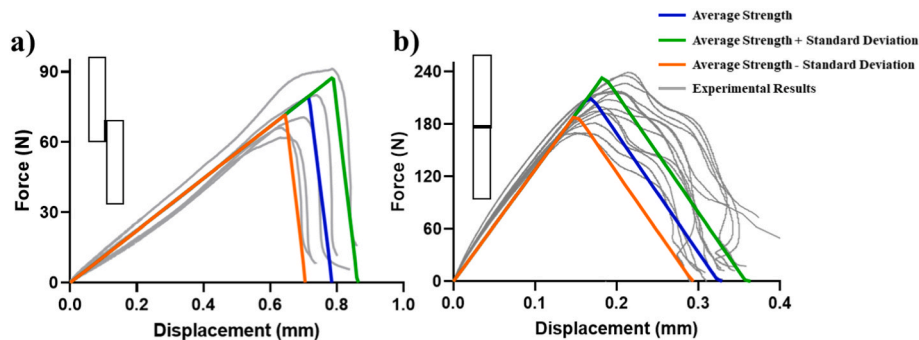


Fig. 10. Experimental results (grey) for the a) SLJ tests and b) LTT tests. To capture the calibrated strength distribution, the CZM law with the average strength (blue), the average strength plus one standard deviation (green) and the average strength minus one standard deviation (orange) are included in each plot. (For interpretation of the references to colour in this figure legend, the reader is referred to the Web version of this article.)

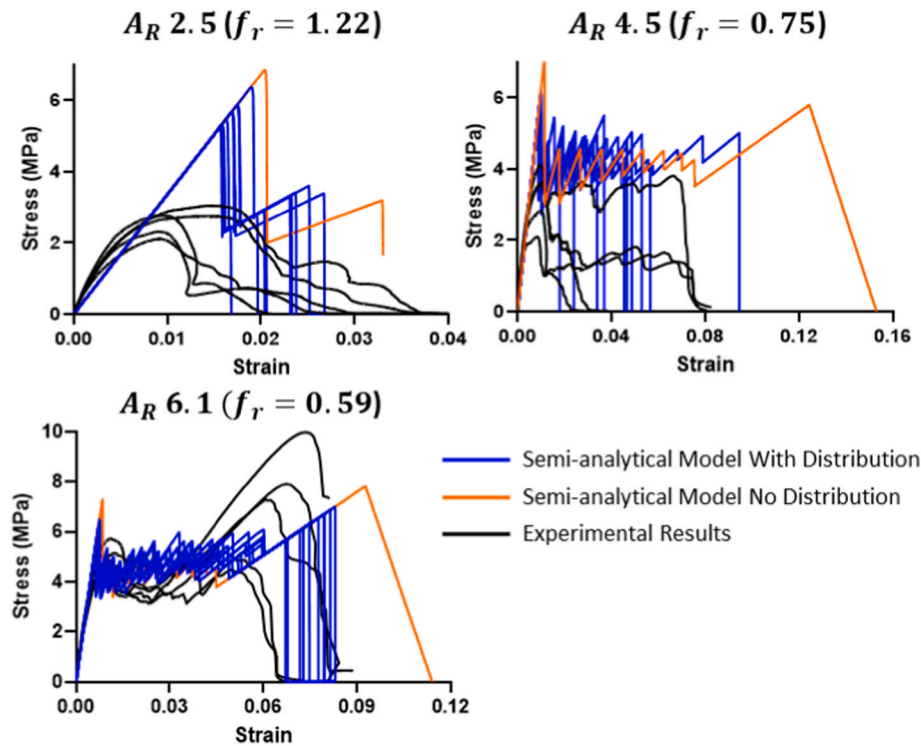


Fig. 11. Stress-strain response comparison for Brick-and-Mortar structure experimentally tested (black) and simulated with the semi-analytical model with and without a strength distribution (blue and orange, respectively) for A_R of 2.5, 4.5 and 6.1. (For interpretation of the references to colour in this figure legend, the reader is referred to the Web version of this article.)

4.2. Comparison of semi-analytical model and experiments

Based on the CZM parameters for TB+, we calculate the f_r value (using Equation (8)) to be 1.22, 0.75 and 0.59 for A_R of 2.5, 4.5 and 6.1, respectively. Without a distribution, we therefore predict the structures with A_R of 4.5 and 6.1 to exhibit ‘peak-plateau-peak’ failure and the structure with A_R of 2.5 to exhibit ‘two-peak’ failure. This is confirmed in the semi-analytical model of the structures without a distribution, see the orange plots in Fig. 11.

Once the strength distribution is included, see the blue curves in Fig. 11, the model predicts that the structure closest to the transition point (i.e. A_R of 4.5) will drop down to ‘peak-plateau’ or ‘two-peak’ failure, and there will be a subsequent large variation in the strain to failure, while the structures with A_R of 6.1 is predicted to remain within the ‘peak-plateau-peak’ failure regime and the structure with an A_R of 2.5 is predicted to remain within the ‘two-peak’ failure regime.

Significantly, the failure regimes predicted by the semi-analytical model with a strength distribution in the layer matches the experimental results, see the black curves in Fig. 11. That is, simulated structures with A_R of 4.5 exhibit a range of failure regimes, resulting in a broad range of predicted strain to failure, while all other structures exhibit a single failure regime type. Snapshots of the experiments at the point the shear layers begin to fail (i.e. at the final peak in the stress-strain response) are provided in Fig. 12 to further demonstrate the range of failure regime types exhibited by structures with A_R of 4.5. Snapshots of the structures with A_R of 6.1, which exhibits ‘peak-plateau-peak’ failure in all experimental tests, are also included in Fig. 12 for comparison. In these snapshots, we can clearly see that the structures with A_R of 6.1 are able to completely distribute damage through all the normal layers before full failure (indicative of ‘peak-plateau-peak’ failure), while the number of normal layers that fail prior to full failure varies for structures with A_R of 4.5 (indicative of a range of failure regimes). Comparison of the semi-analytical model and experimental results also shows that incorporating the realistic variability of the

strength of the layer improves the prediction of the yield stress.

Therefore, by incorporating the realistic strength distribution into the Brick-and-Mortar model we considerably improve our prediction of the range of failure regimes the structure will exhibit, the range in the strain to failure and the prediction of the yield stress. This highlights the practical importance of understanding the effect of layer strength variability and incorporating layer strength variability into models of the Brick-and-Mortar structure.

Overall, the semi-analytical model is quite remarkable in capturing the experimental response, given the simplicity of the model. The main discrepancy observed is in the yield stress for smaller aspect ratios. More generally, model predictions are far from experiments at low aspect ratio but get closer to experiments when the aspect ratio increases. This can be explained in the following way. The main simplification of our model is to replace the real complex stress field by a highly simplified one, with a uniform normal or shear stress in layers and neglecting stress at the junction between layers. The assumed stress field may be realistic far away from layer junctions, but not at junctions. When the aspect ratio increases, the fraction of junction regions decreases. Our model is therefore more accurate in the case of high aspect ratios. Improving the quantitative predictions of the model to better capture the yield stress for structures with smaller aspect ratios will be a subject of future work. This may include, for example, extending the model to consider more realistic traction-separation laws in the CZM, such as incorporating strain hardening (Abid et al., 2018, 2019) or utilising exponential damage laws (Wilbrink et al., 2010).

Including the deformation of the bricks is in principle possible within our semi-analytical framework. It would result in a slight decrease in the slope of the initial stress-strain curve, due to the deformation of the brick contributing to the average strain of the composite. Brick failure would only occur if the brick strength were lower than both the normal layer strength and the shear layer strength (Begley et al., 2012), leading to sudden failure partway through the elastic response. However, this scenario was never observed in our experiments and therefore we did

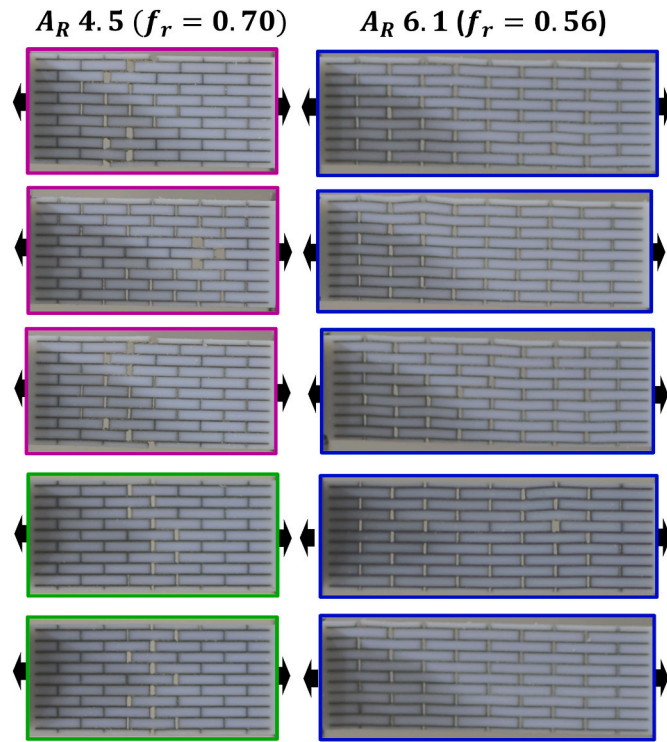


Fig. 12. Snapshots of the experimental uniaxial tension tests at the point the shear layers begin to fail (i.e., at the final peak in the stress-strain response) for the structures with A_R of 4.5 and 6 to demonstrate the distribution of damage through the normal layers prior to shear layer failure. All five structures that were experimentally tested are included. Snapshots are highlighted in green if they exhibit ‘two-peak’ failure (damage is distributed to two to three rows of normal layers prior to full failure), purple if they exhibit ‘peak-plateau’ (damage is distributed to more than three, but not to all, normal layers prior to full failure) and blue if they exhibit ‘peak-plateau-peak’ failure (damage is distributed to all normal layers prior to full failure). (For interpretation of the references to colour in this figure legend, the reader is referred to the Web version of this article.)

not consider deformation and failure of the bricks in our study.

5. Conclusions

The present study explored the effect of strength variability on the failure regimes and mechanical properties of Brick-and-Mortar structures with a finite size representative of the size printable with Additive Manufacturing. To do this, the semi-analytical model of finite-size Brick-and-Mortar structures that was previously developed by our group was extended to incorporate a distribution in the strength of the layers. The study revealed that a distribution in the strength of the layers has a significant effect on the failure regimes, and subsequently on the mechanical properties, of the structure. The main conclusions of this study are the following:

- For a structure without variability in layer strength, we have shown in our previous work (Hunter et al., 2021) that different failure regimes could occur, depending on the value of the dimensionless parameter f_r :

$$f_r = \frac{1}{\sigma_R} \left(\frac{1}{2E_R} + \frac{1}{A_R} + \frac{1}{2(E_R + A_R)} \right)$$

where $f_r = 1$ is at the transition point, $f_r < 1$ corresponds to the ‘peak-plateau-peak’ regime and $f_r > 1$ corresponds to the ‘two-peak’ regime. The key novel finding of this work is that the parameter f_r also controls the probability of a structure to change its failure regime in the presence

of layer strength variability. Specifically, we have shown that a structure that exhibits the favourable ‘peak-plateau-peak’ failure regime in the absence of strength variability ($f_r < 1$) has a probability to transition to the inferior ‘peak-plateau’ or ‘two-peak’ failure regimes when a variability in the layer strength is introduced. For a given layer strength distribution, the probability of this transition to take place increases as f_r gets closer to 1. Conversely, for a given $f_r < 1$, the transition probability increases with the variability (i.e. the standard deviation) of the distribution.

- The significance of a change of failure regime induced by introducing a layer strength variability is best seen in the drop in the average strain to failure and simultaneous increase in strain to failure variability. We further showed that the dimensionless parameter f_r also dictates how the strain to failure changes with changing the variability in the material properties. To the best of our knowledge, the relationships between structure parameters (via f_r), strength variability, and strain to failure have not been systematically investigated before.
- Introducing a variability in the normal layer strength in the model induces a decrease in the yield stress, while introducing a variability in the shear layer strength has no impact on this property. While this finding may seem predictable or trivial, it is nevertheless significant because it contradicts the findings of previous studies (Luo et al., 2017, 2018), which found the yield stress to be affected by the shear layer strength. The contradiction is due to these previous studies ignoring the normal layers in their model. Our study therefore demonstrates the importance of including the normal layers for realistic simulations of the mechanical response of Brick-and-Mortar structures. The relative decrease in yield stress with increasing normal layer variability is further shown to be independent of the dimensionless parameter f_r .

Our findings are important for the design of Brick-and-Mortar structures which exhibit the more favourable ‘peak-plateau-peak’ failure regime, as well as controlled yield stress and strain-to-failure, taking the inherent material variability into account. They also signify the importance of incorporating strength variability of the layer material into models to accurately predict the failure regimes of the structure and its subsequent mechanical properties.

To demonstrate the practical importance of capturing layer strength variability in models of Brick-and-Mortar structures, we further developed a novel method to incorporate the variability in layer strength measured experimentally via simple tests into CZMs with strength distribution. Once calibrated, the CZMs were used as such in our semi-analytical model to predict the structure response, with no further calibration or fitting. By incorporating the realistic strength distribution into the Brick-and-Mortar model, we considerably improved our prediction of 1) the range of failure regimes the structure will exhibit, 2) the range in the strain to failure and 3) the prediction of the yield stress, as compared to the predictions of the model without strength variability. To the best of our knowledge, this is the first time that theoretical predictions of the effect of strength variability on the structure response have been directly validated experimentally. Future improvements of the model could include the implementation of CZMs with strength variability in finite element simulations, as well as the consideration of refined traction-separation and damage evolution laws, and the exploration of other strength distributions.

Author agreement statement

G. Hunter: Conceptualization, Methodology, Software, Formal Analysis, Investigation, Writing - Original Draft. **L. Djumas:** Conceptualization, Methodology, Formal Analysis, Writing - Review & Editing. **A. Molotnikov:** Conceptualization, Methodology, Formal Analysis, Writing - Review & Editing, Supervision. **L. Brassart:**

Conceptualization, Methodology, Formal Analysis, Writing - Review & Editing, Supervision.

Declaration of competing interest

The authors declare that they have no known competing financial interests or personal relationships that could have appeared to influence the work reported in this paper.

Data availability

Data will be made available on request.

Acknowledgements

This research was supported by an Australian Government Research Training Program (RTP) Scholarship, the ATSE Ezio Rizzardo Scholarship and by additional funding from Monash University.

References

- Abid, N., Mirkhalaf, M., Barthelat, F., 2018. Discrete-element modeling of nacre-like materials: effects of random microstructures on strain localization and mechanical performance. *J. Mech. Phys. Solid.* 112, 385–402.
- Abid, N., Pro, J.W., Barthelat, F., 2019. Fracture mechanics of nacre-like materials using discrete-element models: effects of microstructure, interfaces and randomness. *J. Mech. Phys. Solid.* 124, 350–365.
- Anup, S., 2015. Influence of initial flaws on the mechanical properties of nacre. *J. Mech. Behav. Biomed. Mater.* 46, 168–175.
- Askarinejad, S., Rahbar, N., 2015. Toughening mechanisms in bioinspired multilayered materials. *J. R. Soc. Interface* 12 (102), 20140855.
- Askarinejad, S., et al., 2018. Effects of tablet waviness on the mechanical response of architected multilayered materials: modeling and experiment. *Compos. Struct.* 195, 118–125.
- Askarinejad, S., Shalchy, F., Rahbar, N., 2021. Role of interphase layers in mechanical properties of nacreous structures. *Compos. B Eng.* 225, 109255.
- Barclift, M., Williams, C., 2012. Examining variability in the mechanical properties of parts manufactured via polyjet direct 3D printing. In: 23rd Annual International Solid Freeform Fabrication Symposium - an Additive Manufacturing Conference. SFF, 2012.
- Barthelat, F., et al., 2006. Mechanical properties of nacre constituents and their impact on mechanical performance. *J. Mater. Res.* 21 (8), 1977–1986.
- Barthelat, F., et al., 2007a. On the mechanics of mother-of-pearl: a key feature in the material hierarchical structure. *J. Mech. Phys. Solid.* 55 (2), 306–337.
- Barthelat, F., Espinosa, H.D., 2007b. An experimental investigation of deformation and fracture of nacre-mother of pearl. *Exp. Mech.* 47 (3), 311–324.
- Bass, L., Meisel, N.A., Williams, C.B., 2016. Exploring variability of orientation and aging effects in material properties of multi-material jetting parts. *Rapid Prototyp. J.* 22 (5), 826–834.
- Begley, M.R., et al., 2012. Micromechanical models to guide the development of synthetic 'brick and mortar' composites. *J. Mech. Phys. Solid.* 60 (8), 1545–1560.
- Bekah, S., Rabiei, R., Barthelat, F., 2012. The micromechanics of biological and biomimetic staggered composites. *JBE* 9 (4), 446–456.
- Bonderer, L.J., Feldman, K., Gauckler, L.J., 2010a. Platelet-reinforced polymer matrix composites by combined gel-casting and hot-pressing. Part I: polypropylene matrix composites. *Compos. Sci. Technol.* 70 (13), 1958–1965.
- Bonderer, L.J., Feldman, K., Gauckler, L.J., 2010b. Platelet-reinforced polymer matrix composites by combined gel-casting and hot-pressing. Part II: thermoplastic polyurethane matrix composites. *Compos. Sci. Technol.* 70 (13), 1966–1972.
- Cazón, A., Morer, P., Matey, L., 2014. PolyJet technology for product prototyping: tensile strength and surface roughness properties. *Proc. IME B J. Eng. Manufact.* 228 (12), 1664–1675.
- Chintapalli, R.K., et al., 2014. Strain rate hardening: a hidden but critical mechanism for biological composites? *Acta Biomater.* 10 (12), 5064–5073.
- Deville, S., et al., 2006. Freezing as a path to build complex composites. *Science* 311 (5760), 515–518.
- Dimas, L.S., et al., 2013. Tough composites inspired by mineralized natural materials: computation, 3D printing, and testing. *Adv. Funct. Mater.* 23 (36), 4629–4638.
- Dimas, L.S., Buehler, M.J., 2014. Modeling and additive manufacturing of bio-inspired composites with tunable fracture mechanical properties. *Soft Matter* 10 (25), 4436–4442.
- Djumas, L., et al., 2016. Enhanced mechanical performance of bio-inspired hybrid structures utilising topological interlocking geometry. *Sci. Rep.* 6, 26706.
- Frølich, S., et al., 2017. Uncovering nature's design strategies through parametric modeling. Multi-Material 3D Printing, and Mechanical Testing Advanced Engineering Materials 19 (6), 201600848.
- Gehrke, N., et al., 2005. Retrosynthesis of nacre via amorphous precursor particles. *Chem. Mater.* 17 (26), 6514–6516.
- Gu, G.X., et al., 2016. Biomimetic additive manufactured polymer composites for improved impact resistance. *Extreme Mechanics Letters* 9, 317–323.
- Gu, G.X., et al., 2017a. Printing nature: unraveling the role of nacre's mineral bridges. *J. Mech. Behav. Biomed. Mater.* 76, 135–144.
- Gu, G.X., Takaffoli, M., Buehler, M.J., 2017b. Hierarchically enhanced impact resistance of bioinspired composites. *Adv. Mater.* 29 (28), 1700060.
- Hunter, G., et al., 2021. Controlling failure regimes in Brick-and-Mortar structures. *Extreme Mechanics Letters*, 101596.
- Hunter, G., et al., 2022. Effect of angled layers on failure regimes in brick-and-mortar structures. *Mater. Des.* 218, 110680.
- Kęsy, A., Kotliński, J., 2010. Mechanical properties of parts produced by using polymer jetting technology. *Arch. Civ. Mech. Eng.* 10 (3), 37–50.
- Khalid, G.A., et al., 2020. Material response characterization of three poly jet printed materials used in a high fidelity human infant skull. *Mater. Today: Proc.* 20, 408–413.
- Launey, M.E., et al., 2009. Designing highly toughened hybrid composites through nature-inspired hierarchical complexity. *Acta Mater.* 57 (10), 2919–2932.
- Libonati, F., et al., 2016. Bone-Inspired Materials by Design: Toughness Amplification Observed Using 3D Printing and Testing Advanced Engineering Materials 18 (8), 1354–1363.
- Luo, W., Bažant, Z.P., 2017. Fishnet model for failure probability tail of nacre-like imbricated lamellar materials. *Proc. Natl. Acad. Sci. USA* 114 (49), 12900–12905.
- Luo, W., Bažant, Z.P., 2018. Fishnet model with order statistics for tail probability of failure of nacreous biomimetic materials with softening interlaminar links. *J. Mech. Phys. Solid.* 121, 281–295.
- Mirzaeifar, R., et al., 2015. Defect-tolerant bioinspired hierarchical composites: simulation and experiment. *ACS Biomater. Sci. Eng.* 1 (5), 295–304.
- Mueller, J., Shea, K., Darao, C., 2015. Mechanical properties of parts fabricated with inkjet 3D printing through efficient experimental design. *Mater. Des.* 86, 902–912.
- Munch, E., et al., 2008. Tough, bio-inspired hybrid materials. *Science* 322 (5907), 1516–1520.
- Oaki, Y., Imai, H., 2005. The hierarchical architecture of nacre and its mimetic material. *Angew. Chem. Int. Ed.* 44 (40), 6571–6575.
- Oner Ekiz, O., Dericioglu, A.F., Kakisawa, H., 2009. An efficient hybrid conventional method to fabricate nacre-like bulk nano-laminar composites. *Mater. Sci. Eng. C* 29 (6), 2050–2054.
- Pro, J.W., et al., 2015. The impact of stochastic microstructures on the macroscopic fracture properties of brick and mortar composites. *Extreme Mechanics Letters* 5, 1–9.
- Slesarenko, V., et al., 2017a. Understanding the strength of bioinspired soft composites. *Int. J. Mech. Sci.* 131–132, 171–178.
- Slesarenko, V., Kazarinov, N., Rudykh, S., 2017b. Distinct failure modes in bio-inspired 3D-printed staggered composites under non-aligned loadings. *Smart Mater. Struct.* 26 (3), 035053.
- Song, F., Soh, A.K., Bai, Y.L., 2003. Structural and mechanical properties of the organic matrix layers of nacre. *Biomaterials* 24 (20), 3623–3631.
- TangoPlus Datasheet. Stratasys Ltd.
- Vero Material Datasheet. Stratasys Ltd.
- Wang, C.-a., et al., 2000. Biomimetic structure design — a possible approach to change the brittleness of ceramics in nature. *Mater. Sci. Eng. C* 11 (1), 9–12.
- Wilbrink, D.V., et al., 2010. Scaling of strength and ductility in bioinspired brick and mortar composites. *Appl. Phys. Lett.* 97 (19), 193701.
- Yan, Y., et al., 2022. Nacre's brick-mortar structure suppresses the adverse effect of microstructural randomness. *J. Mech. Phys. Solid.* 159, 104769.
- Yang, W., et al., 2019. Strength analysis of bio-inspired composites reinforced by regularly and randomly staggered platelets. *Compos. Struct.* 216, 415–426.
- Zhang, Z.Q., et al., 2010. Mechanical properties of unidirectional nanocomposites with non-uniformly or randomly staggered platelet distribution. *J. Mech. Phys. Solid.* 58 (10), 1646–1660.
- Zhang, P., Heyne, M.A., To, A.C., 2015. Biomimetic staggered composites with highly enhanced energy dissipation: modeling, 3D printing, and testing. *J. Mech. Phys. Solid.* 83, 285–300.